

Inspectability and printability of lines and spaces halftone masks for the advanced DRAM node

Arndt C. Dürr^{a,*}, Karsten Gutjahr^b, Jan Heumann^a, Martin Stengl^a, Frank Katzwinkel^b,
Andreas Frangen^b, Thomas Witte^a

^aAdvanced Mask Technology Center (AMTC), Rähnitzer Allee 9, 01109 Dresden, Germany
^bQimonda Dresden GmbH & Co. OHG, Königsbrücker Straße 180, 01099 Dresden, Germany

ABSTRACT

With decreasing pattern sizes the absolute size of acceptable pattern deviations decreases. For mask-makers a new technology requires a review, which mask design variations print on the wafer under production illumination conditions and whether these variations can be found reliably (100%) with the current inspection tools. As defect dispositioning is performed with an AIMS-tool, the critical AIMS values, above which a defect prints lithographically significant on the wafer, needs to be determined. In this paper we present a detailed sensitivity analysis for programmed defects on 2 different KLA 5xx tools employing the pixel P90 at various sensitivity settings in die-to-die transmitted mode. Comparing the inspection results with the wafer prints of the mask under disar illumination it could be shown that all critical design variations are reliably detected using a state-of-the-art tool setup. Furthermore, AIMS measurements on defects with increasing defect area of various defect categories were taken under the same illumination conditions as for the wafer prints. The measurements were evaluated in terms of AIMS intensity variation (*AIV*). It could be shown that the AIMS results exhibit a linear behavior if plotted against the square-root area (*SRA*) of the defects on the mask as obtained from mask SEM images. A consistent lower *AIV* value was derived for all defect categories.

Keywords: AIMS, mask inspection, defect disposition, aerial imaging, defect printability, optical imaging, 193nm lithography, mask, reticle

1. INTRODUCTION

For the production of “defect free” masks defect printability studies play a key-role. With the tremendous prices of new inspection tools it is a significant cost-factor whether a new mask technology requires capability-wise a new inspection tool with improved capability or if all lithographically significant defects are reliably captured by tuning the sensitivity of an already installed inspection tool. On the other hand, capturing lithographically uncritical defects employing excessive sensitivity might influence the mask’s cycle time and even the mask yield due to unnecessary repairs. Thus, defect printability studies are carried out first to evaluate the capability of expensive inspection tools and show potential to extend their usability for upcoming technologies and secondly to tune the sensitivity settings preferably such that only lithographically significant defects are captured improving the mask production yield.

Aerial imaging microscopy (AIMS) measurements under stepper illumination conditions are commonly used to judge whether a defect is lithographically significant printing or if a defect is uncritical.^{1,2} This assessment is based upon a correlation between AIMS measurement results and wafer prints of production relevant programmed defects of various sizes and shapes.

Previous printability studies for lines-and-spaces (l&s) structures for the 70nm node indicated that the capability of the pixel P90 to reliably capture critical defects printed under disar- and quasar illumination is at the limit for most and even insufficient for several defect types (e.g., “undersize”-defects, clear and dark center defects). In addition, it was found difficult to precisely assess the size limit for which a given defect type is lithographically significant printing on the wafer. Finally, the results of the AIMS measurements scattered strongly

*Further author information: (Send correspondence to Arndt C. Dürr)
E-mail: Arndt.Duerr@amtc-dresden.com, Telephone: +49 (0) 351 4048 268

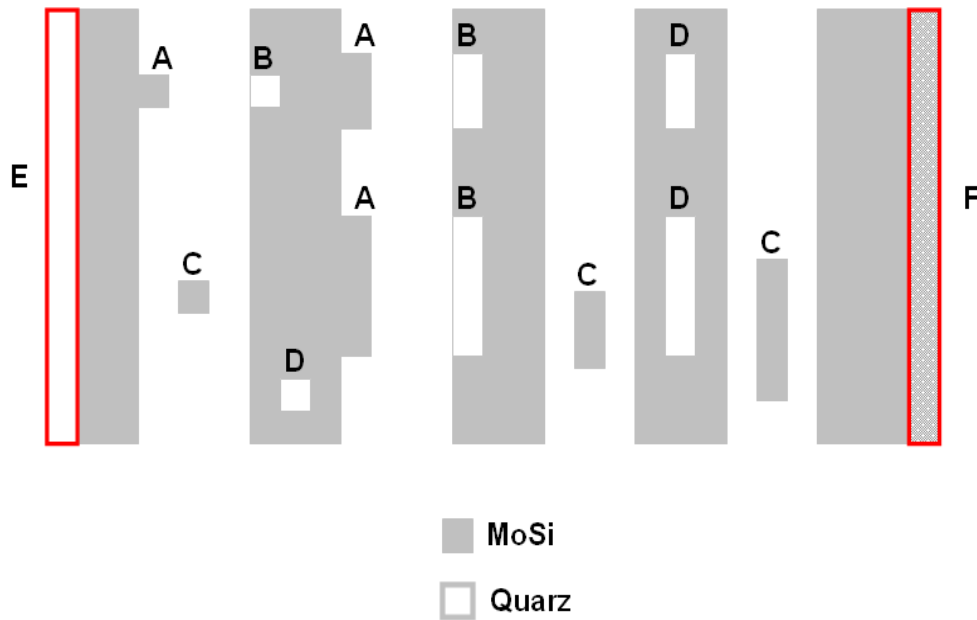


Figure 1. Layout of the tight l&s-pattern with programmed defects. The letters refer to the different defect types (partially with 3 different aspect ratios of 1:1, 1:2, and 1:5). A: dark extension (DEX) with 3 different aspect ratios. B: clear extension (CEX) with 3 different aspect ratios. C: dark center (DCE) with 3 different aspect ratios. D: clear center (CCE) with 3 different aspect ratios. E: under sizing (UNDER). F: over sizing (OVER).

if plotted against the measured square root of the area A (SRA) of the defect on the mask and therefore did not allow for an accurate determination of an AIMS threshold that reliably indicates whether a defect prints critically or not.³

Thus, in the present study for DRAM l&s-structures below the 70nm node the important question is investigated if the pixel P90 is still sufficient or if the delivery of “defect free” masks for this technology is gated by the availability of the P72 and puts additional costs to the mask making process. Furthermore, the correlation between wafer prints and AIMS measurement results has been investigated to determine the AIMS result for the smallest printing defect for the various defect shapes and types.

2. EXPERIMENTAL

For the present study a MoSi 193nm mask with programmed defects at tight lines and spaces (l&s) structures in one chip is used. The design contains:

- 14 different defect categories
- 20 different defect sizes within each defect category

A second chip with identical but defect-free structures is used as reference structure for die-to-die inspections. Figure 1 displays a schematic of the various defect categories.

The programmed defect pattern was inspected against the defect free pattern in die-to-die transmission (D2DT) mode using the P90 detection pixel. 3 different sensitivity settings for the respective detectors HiRes1 and HiRes2 were evaluated (90/90, 95/95, and 100/100, respectively) at two KLA5xx tools (one at AMTC and one at Qimonda). Each inspection was repeated 10 times to allow for a statistically based sensitivity analysis of the employed inspection settings. In the sensitivity analysis the KLA-triggered positions of defects are correlated

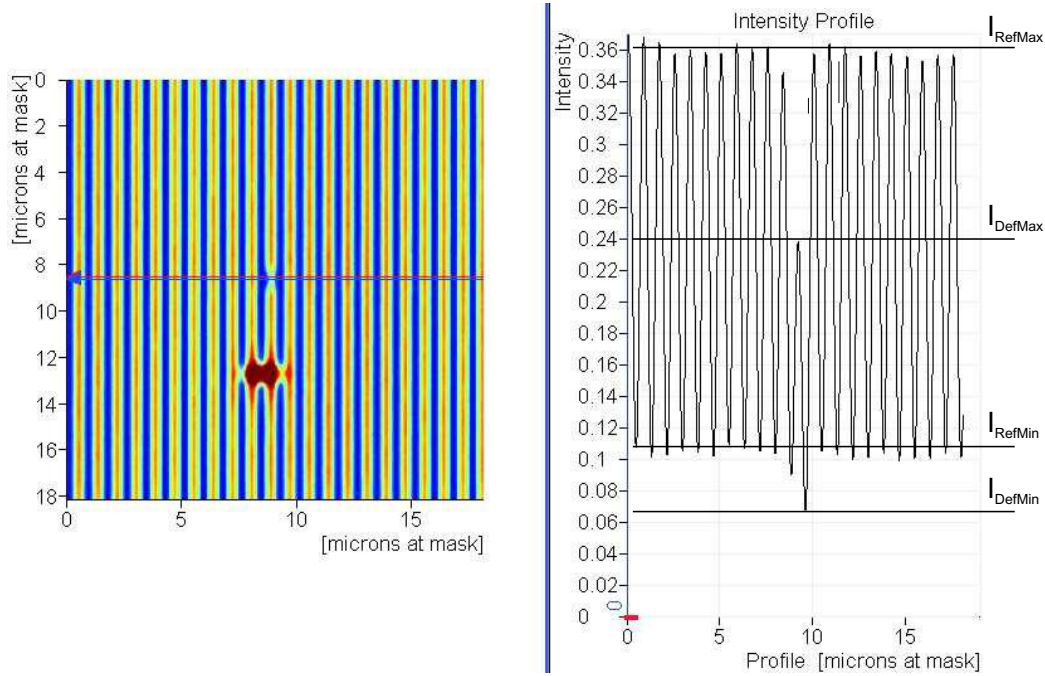


Figure 2. AIMS image of a defect in a lines and spaces pattern on a programmed defect mask and a profile along the line (left-hand side). The corresponding intensity profile is shown on the right hand side. The principle of determining I_{RefMax} , I_{DefMax} , I_{RefMin} , and I_{DefMin} is displayed. *Note*, that the large bright structure $4\mu\text{m}$ below the defect is a defect marker.

to their programmed coordinates. The matching range was set to $10\mu\text{m}$ to ensure that only programmed defects are used for the correlation.

The chip with programmed defects was printed on a wafer using disar illumination conditions. Subsequently, wafer CD SEM images were taken at the programmed defect sites. Based on the wafer CD SEM images for each defect category the programmed defects were classified as “uncritical design variation” and as “printing defect”, respectively. The smallest “printing defect” for each defect category is considered as “print threshold” in the following sensitivity- and AIMS-analysis.

AIMS measurements of the programmed defects were carried out under the same illumination conditions as the wafer prints, i.e., disar illumination. An AIMSTM 193i tool at the AMTC was used for these measurements.⁴⁻⁶ To quantify the transmission deviation of a programmed defect at first the largest transmission deviation in the AIMS image was identified. Subsequently, the deviation of the intensity profile along a cross-section over the defect in the maximum and the minimum, respectively, was calculated employing Eq. (1) and (2), see also Fig. 2. All defects have been evaluated manually.⁷

$$MaxTrans = \left(\frac{I_{DefMax}}{I_{RefMax}} - 1 \right) \times 100\% \quad (1)$$

$$MinTrans = \frac{I_{DefMin} - I_{RefMin}}{I_{RefMax} - I_{RefMin}} \times 100\%. \quad (2)$$

The worst of both absolute values was then assigned to the defect as AIMS Intensity Variation (AIV):

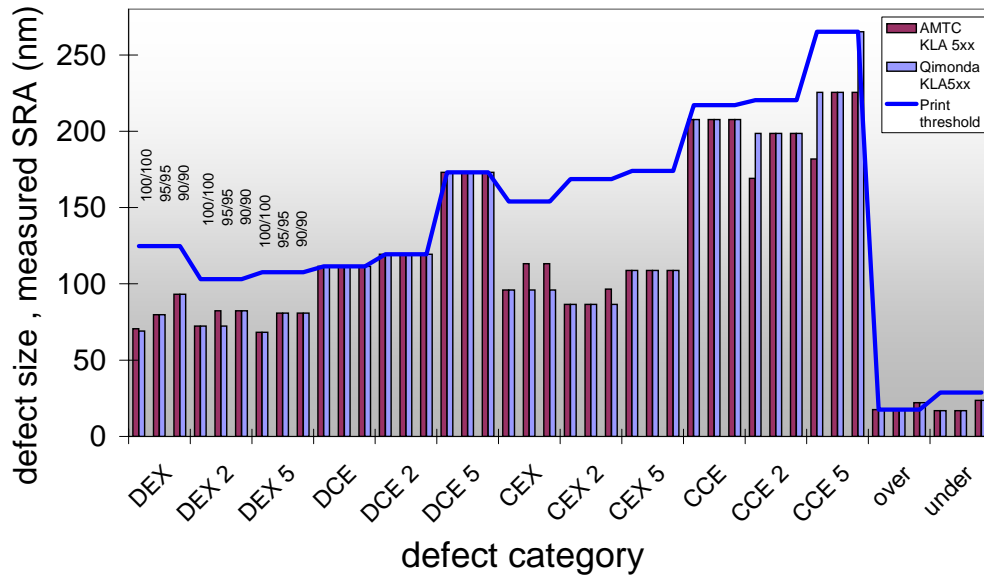


Figure 3. Bars: Inspection capability for 2 different KLA5xx tools at 3 different sensitivity settings for the investigated defect categories. The bars cover the defect sizes (measured *SRA*) that were detected with < 100% capture rate, i.e., all defects above the bars are captured 100%. Solid line: The solid line represents the print threshold (measured *SRA*) for the various defect categories, i.e., all defects laying above the solid line are critically printing on the wafer. Bars ending beneath the solid line indicate that all critical printing defects are captured 100%. However, the larger the gap beneath the solid line to a bar’s end the more uncritical defects are captured and need to be classified and will potentially be repaired.

$$AIV = \max(|MaxTrans|, |MinTrans|). \quad (3)$$

Reticle CD SEM images were taken of the programmed defects with a Holon EMU 220A CD SEM tool. The area *A* of the defects was determined using the image processing software “KLA ProData” of KLA Tencor. The square root of the area *A*, hereafter referred to as *SRA*, was then calculated. It represents an one-dimensional defect size, independent of the aspect ratio of the various defect categories. The *AIV* (Eq. 3) was then plotted as a function of the *SRA*.

3. RESULTS AND DISCUSSION

3.1. Inspection: sensitivity analysis correlated to wafer prints

Figure 3 shows the sensitivity results for the KLA5xx tools at AMTC and Qimonda for all 14 defect categories at the 3 different sensitivity settings (100/100, 95/95, and 90/90). The bars in the diagram indicate the range of defect sizes (measured *SRA*) on mask that are not detected with 100% capture rate. In turn all defects sizes outside the bar exhibit a capture rate of 100%. The print threshold for each defect category has been determined by CD SEM image review of the defects on the wafer prints. All defects of a given defect category with sizes above the line are considered as critically printing and vice versa. Hence, to ensure that all critically printing defects are 100% captured it is required that the bars don’t exceed the print threshold line.

It can be clearly seen in Fig. 3 that for identical tool settings the sensitivity of the two tools is comparable. It should be noted that within one defect type (dark or clear extension) the sensitivity with respect to defect size is very similar. On the contrary the printing behavior of one defect type clearly depends on the defect shape (DEX vs. DEX2, DEX5).

In order to capture all critically printing defects utilizing the P90 pixel in conjunction with D2DT sensitivity settings of 100/100 and 95/95 is sufficient. The printing behavior of the oversize defects avoids the KLA5xx tools to be run at the more relaxed sensitivity settings of 90/90. In general, isolated defects (clear and dark), here referred to as “center defects”, are more difficult to detect than on-edge defects. There are mainly two explanations in the community.

1. Small isolated structures are usually more severely influenced by the manufacturing process than on-edge defects. Typically, their edges are more rounded and they do not exhibit the full height. In particular, the smaller height significantly increases the transmission making it much more difficult to detect.
2. For clear isolated defects the image contrast inversion experienced with decreasing defect size jeopardizes their detectability.

From a manufacturing perspective, center and over-/undersize defects are comparatively unlikely to occur. Center defects are less likely to occur in tight l&s-patterns at this small half-pitch since any resist defect would more likely result either in extensions or even bridging defects. Also it is unlikely in real mask manufacturing to find an “isolated” oversize defect (only one line affected) of uniform CD-deviation along the entire line. Upon occurrence oversize defects affect bundles of lines. Thus, oversize defects in manufacturing will most likely be detected more easily than the inspection results might imply.

Nevertheless, to ensure safe capturing of all critical defects the results suggest application of full sensitivity in the manufacturing process. The trade-off setting the tools to full sensitivity is that the tool works at its limit. Also, for other defect categories not lithographically relevant defects are captured. This might result in a higher defect count and impact the cycle-time by additional repairs or even the yield.

3.2. AIMS analysis of defects

Figure 4 shows the AIMS intensity variation values as a function of the measured mask *SRA* for dark and clear extension defects with various aspect ratios. Figure 5 illustrates the AIMS intensity variation as a function of the measured CD variation ΔCD of the line from the nominal CD. In all graphs printing defects are denoted as triangles whereas not lithographically significant printing defects are represented by squares. The defect at the print threshold is symbolized by a circle.

For all displayed defect classes in Figs. 4 and 5 the AIMS values correlate very well linearly with the *SRA* and ΔCD , respectively, over a large defect size range. This observation is the result of a mature manufacturing process with high pattern fidelity (e.g., neglectable line edge roughness, defect shape conservation even for small defects, etc.), of the application of aggressive illumination conditions that ensure a sufficient pattern contrast and of the application of an AIMS tool with a high measurement accuracy.^{4,6} *Note*, that the linear correlation range covers for all defect categories uncritical and critically printing defects and thus includes the defect size at the printing threshold. This allows to reliably determine the *AIV* within a given defect category for arbitrary defects sizes in this range by linear inter-/extrapolation, being useful particularly in the vicinity of the print threshold. Previous printability studies for halftone material and chrome-less phaseshift masks for 75 nm half-pitch (1x) showed more data scattering. This was owed to the overall mask manufacturing process as well as to a predecessor AIMS tool and complicated the determination of an *AIV* value at an arbitrary *SRA* in the vicinity of the print threshold by extrapolation.^{3,8}

3.2.1. Dark and clear extensions

Figures 4 (a)-(c) show the *AIV* as a function of mask *SRA* for dark extension defects of varying aspect ratios. Figure 4 (a) refers to quadratic defects, DEX (aspect ratio “width into space” : “length parallel to line” = 1:1), (b) and (c) refer to rectangular defects with an aspect ratio of 1:2 (DEX2) and 1:5 (DEX5), respectively. The slope of the linear fit for the 3 different defect types is roughly the same indicating that for dark defects the *AIV* is closely related to the *SRA* and thus almost independent of the defect’s shape. Note however, that the *AIV* at the print threshold for DEX defects is significantly larger than the *AIV* at the print threshold for DEX2 and DEX5 defects (almost the same *AIV* for DEX2 and DEX5). Thus, quadratic dark defects appear to be less

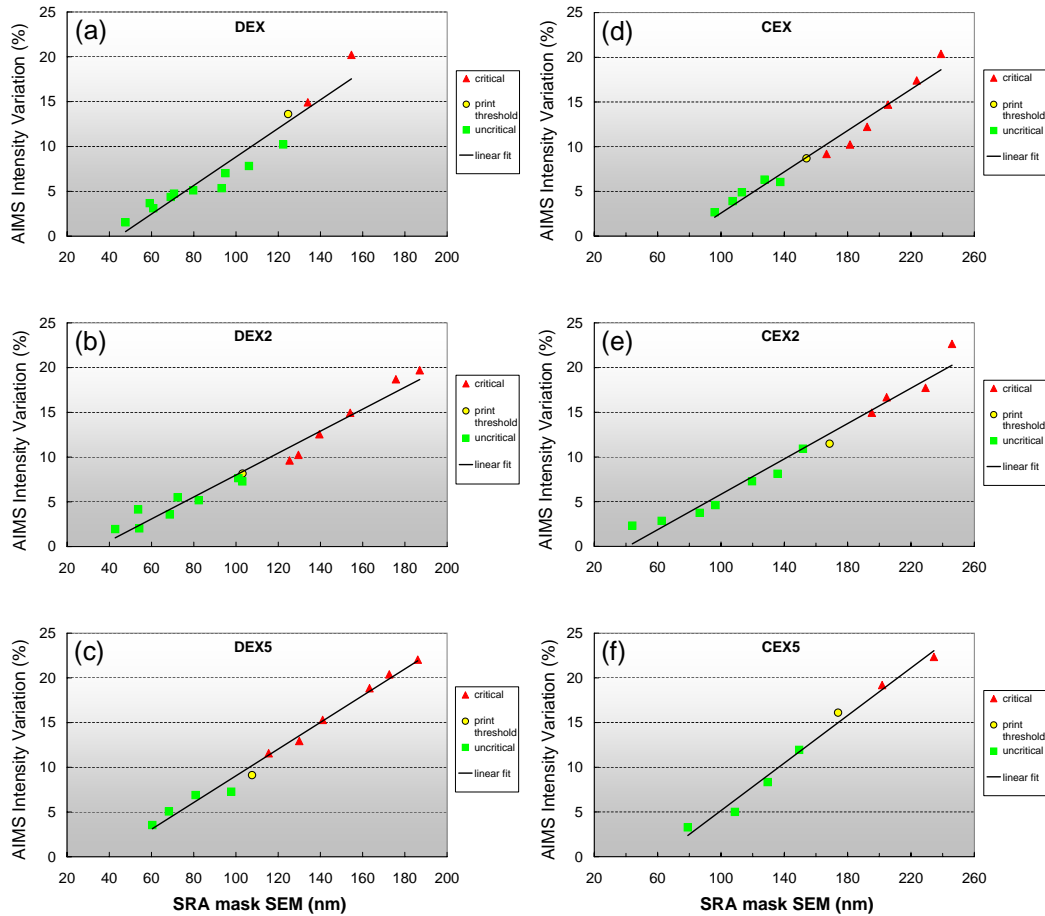


Figure 4. *AIV* values as a function of the measured *SRA* for (a)-(c) dark extensions of various aspect ratios, (d)-(f) clear extensions of various aspect ratios.

critical on masks than rectangular defects since they print lithographically significant only at larger sizes than rectangular dark defects.

Figures 4 (d)-(f) show the *AIV* as a function of mask *SRA* for clear extension defects of varying aspect ratios. Figure 4 (d) refers to quadratic defects, CEX, (e) and (f) refer to rectangular defects with an aspect ratio of 1:2 (CEX2) and 1:5 (CEX5), respectively. For clear extensions, the slope of the linear fit is significantly dependent on the defect's shape, being largest for CEX5 and smallest for CEX2. Currently we have no explanation for this observation. The clear extension defects also show a different behavior than the dark extensions comparing the *AIV* at the respective print threshold. For the CEX defects the *AIV* at the print threshold is smaller than for the rectangular defects. Here, CEX5 exhibits the largest *AIV* at the print threshold. Therefore, within the clear extension class defects with a (nearly) quadratic aspect ratio are the most critical defects.

Comparing the measured *SRA* at the print threshold Fig. 4 shows clearly that the critical *SRA* of clear extension defects is systematically larger than for dark extensions, independent of the defect's aspect ratio. It can not be excluded that this phenomenon is due to the area evaluation process in the imaging processing software "KLA ProData" since the border of a defect is determined based upon a certain gray-scale threshold.

A closer inspection of the *AIV* values of clear and dark extensions shows that the lowest *AIV* values at the print threshold are roughly the same: $AIV_{min}^{dark} = \min(AIV_{DEX}, AIV_{DEX2}, AIV_{DEX5})$ and $AIV_{min}^{clear} =$

$\min(\mathbf{AIV}_{\text{CEX}}, AIV_{\text{CEX}2}, AIV_{\text{CEX}})$ (gating defect categories for AIV_{\min} are marked in bold letters).

Note, that AIV - SRA -plots for center defects are not displayed. Their AIV values at the print threshold are larger than the values of the extension defects, thus, they are not gating the specification requirements. In addition, as mentioned above, in a real manufacturing process center defects are less likely to occur in tight λ -patterns with a similar small half-pitch as present on the investigated mask.

3.2.2. Over- and undersize defects

Figure 5 exhibits the AIV for oversize and undersize defects, respectively, as a function of the measured CD deviation ΔCD from the nominal CD. The slope of both curves is roughly the same. It is clearly seen that the ΔCD for the print-threshold for over-size defects is 35% smaller than for under-size defects. The AIV at the print threshold for over-size defects is only half of the respective AIV for under-size defects. Thus, the oversize defects are more critical for the wafer exposure than the under-size defects.

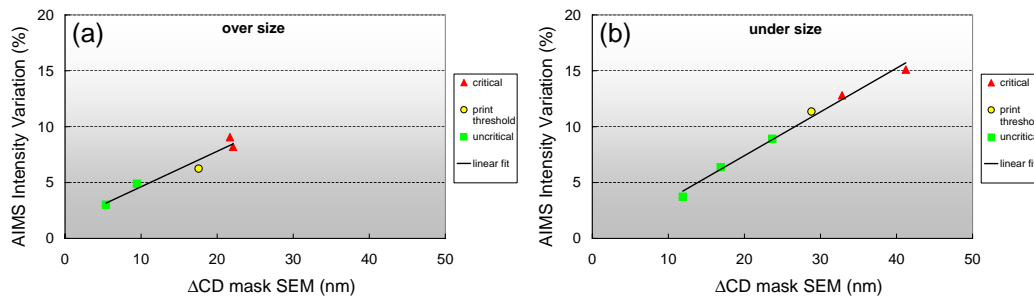


Figure 5. AIV values as a function of ΔCD for (a) oversize and (b) undersize structures.

3.2.3. Summarized AIMS intensity variation at printing threshold

Figure 6 summarizes the AIV values at the print threshold for all defect categories. The graph provides a quick overview over the gating defect shapes within the various defect categories with respect to the AIV value (see also Table 1). The data clearly show that for the investigated technology the oversize defect class has the smallest AIV value at the print threshold of all defect classes and thus is gating the critical AIV value for this technology.

Apart from the over-/undersize defect categories the smallest AIV value at the print threshold is observed for rectangular dark defects with an aspect ratio of 1:2 (DEX2), and an only slightly larger AIV is observed for quadratic clear defects (CEX). All other defect shapes and classes exhibit significantly larger AIV values at the print threshold, in particular the center defects.

Table 1. Gating defect shapes for the various defect categories with respect to the AIV value at the print threshold. The overall gating defect shape (oversize) is emphasizes in bold letters.

defect category	gating shape
dark extensions	DEX2
clear extensions	CEX
dark center	DCE2
clear center	CCE2
over-/undersize	oversize

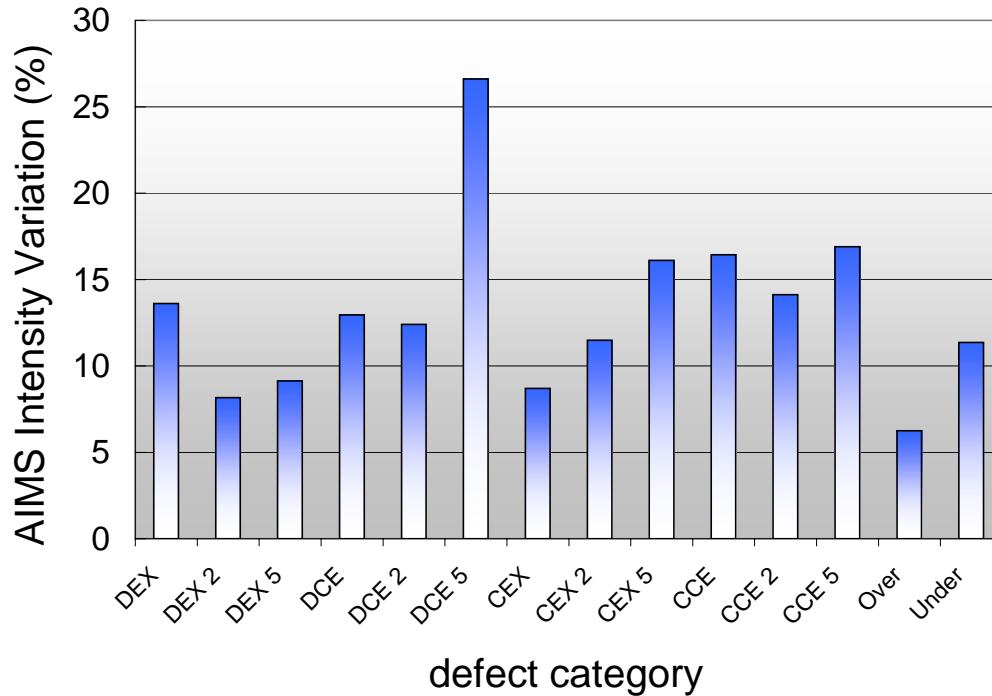


Figure 6. Summary of the *AIV* values at the print threshold for all investigated defect categories.

4. SUMMARY AND CONCLUSIONS

Using a halftone mask with programmed defects in a tight l&s pattern it has been shown that all defects that are critically printing on the wafer are reliably found employing the P90 pixel at 2 different KLA5xx tools independent of the defect category. To ensure a 100% capture rate for oversize defects however, the KLA tools had to be operated not below 95/95 sensitivity settings.

For all investigated extension and over-/undersize defects the AIMS intensity variation *AIV* correlated well linearly with the measured *SRA* (extensions) and ΔCD (over-/undersize), respectively, over a size-range that covered uncritical as well as critical printing defects. This finding allows to reliably interpolate *AIV* values for arbitrary defect sizes in particular in the vicinity of the print threshold. The good linear behavior can be attributed to a mature manufacturing process and the application of an AIMS 193i tool exhibiting high measurement stability. With an *AIV* value of 6.3% at the print threshold the oversize defect category is the gating defect category for the determination of an AIMS limit beneath which all defects are considered to be uncritical.

Since their critical size is so small [$\Delta CD = 7$ nm on mask (!)] that a reliable capturing with pixel P90 is provided only at the full sensitivity of the KLA5xx tools the oversize defects category represent the overall gating defect type for the investigated technology pushing the current tool capabilities (inspection / AIMS) to the limits. Blessing in disguise, “isolated” oversized defects with uniform CD deviation are less likely to be found in real manufacturing.

For the gating defect shape of the – more production relevant – extension defects (the rectangular dark extension with an aspect ratio of 1:2, DEX2) an *AIV* value of 8.2% has been observed.

ACKNOWLEDGMENTS

AMTC is a joint venture of Infineon, AMD and Toppan Photomasks and gratefully acknowledges the financial support by the German Federal Ministry of Education and Research (BMBF) under Contract No. 01M3154A

(“Abbildungsmethodiken für nanoelektronische Bauelemente”).

REFERENCES

1. R. A. Budd, J. Staples, D. B. Dove, “New tool for phase-shift mask evaluation: the stepper equipment aerial image measurement system – AIMS”, Proc. SPIE Vol. 2087, p. 162-171, 1993.
2. R. A. Budd, D. B. Dove, J. L. Staples, R. M. Martino, R. A. Furguson, J. T. Weed, “Development and application of a new tool for lithographic mask evaluation, the stepper equivalent Aerial Image Measurement System, AIMS”, IBM J. Res. Develop. Vol 41 No.1,2 January/March, 1997.
3. K. Eggers, K. Gutjahr, M. Peikert, D. Rutzinger, R. Ludwig, M. Kaiser, A. Dürr, J. Heumann , “Defect printability and inspectability of halftone masks for the 90nm and 70nm node”, Proc. SPIE Vol. 5835, pp. 273-281, 2005.
4. A. M. Zibold, R. Schmid, K. Böhm, R. Brunner, A. C. Dürr, “Application results at 193nm: lithography emulation by aerial imaging and supplementary high resolution measurements”, Proc. SPIE Vol. 5835, p. 115-121, 2005.
5. A. C. Dürr, K. Bubke, M. Sczyrba, S. Angonin, “The importance of being homogeneous: on the influence of illumination inhomogeneity on AIMS images”, Proc. SPIE Vol. 5992, p. 859-872, 2005.
6. A. C. Dürr, A. M. Zibold, K. Böhm “An advanced study for defect disposition through 193 nm aerial imaging”, Proc. SPIE Vol. 6152, p. 895-903, 2006.
7. A. C. Dürr, M. Arndt, J. Fiebig, S. Weiss “Automated evaluation of AIMS images: an approach to minimize evaluation variability”, Proc. SPIE Vol. 6283, 62832A, 2006.
8. J. Heumann, J. Schramm, A. Birnstein, K. T. Park, T. Witte, N. Morgana, M. Hennig, R. Pforr, J. Thiele, N. Schmidt, C. Aquino, “Defect printability and inspectability of Cr-less phase-shift masks for the 70nm node”, Proc. SPIE Vol. 5754, pp. 1022-1028, 2005.